# Evaluation of the role of Au in improving catalytic activity of Ni nanoparticles for the formation of 1-D carbon nanostructures

*Renu Sharma,[1,*] See-Wee Chee,[2,+] Andrew Herzing,[3] Ryan Miranda[4],and Peter Rez[4]*

[1]Center for Nanoscale Science and Technology, National Institute of Science and Technology, Gaithersburg, MD 20899-6203; [2]LeRoy Eyring Center for Solid State Science, Arizona State University, Tempe, AZ 85287, [3]Material Measurement Laboratory, National Institute of Science and Technology, Gaithersburg, MD 20899-8371, [4]Department of Physics, Arizona State University, Tempe, AZ 85287

AUTHOR EMAIL ADDRESS (renu.sharma@nist.gov)

**RECEIVED DATE (to be automatically inserted after your manuscript is accepted if required according to the journal that you are submitting your paper to)**

TITLE RUNNING HEAD: Catalytic activity of Au doped Ni catalyst

CORRESPONDING AUTHOR FOOTNOTE: *Corresponding Author: Renu Sharma, [1]Center for Nanoscale Science and Technology, National Institute of Science and Technology, Gaithersburg, MD 20899-6203. Email: renu.sharma@nist.gov; Ph: +301 9752418; Fax: +301 9755314. [+]Current Address: Materials Research Center, Rensselaer Polytechnic Institute, Troy, NY 12180-3590

ABSTRACT: *In situ* dynamic imaging, using an environmental transmission electron microscope, was employed to evaluate the catalytic activity of $Au/SiO_2$, $Ni/SiO_2$ and $Au\text{-}Ni/SiO_2$ nanoparticles for the formation of 1-D carbon nanostructures such as carbon nanofibres (CNFs) and nanotubes (CNTs). While pure-Au thin-film samples were inactive for carbon deposition at 520 °C in 0.4 Pa of $C_2H_2$, multiwalled CNTs formed from Ni thin films samples under these conditions. The number of nano-particles active for CNF and CNT formation increased for thin films containing 0.1 mole fraction and 0.2 mole fraction of Au, but decreased as the overall Au content in thin-flims was increased above 0.5 mole fraction. Multiwalled CNTs formed with a root growth mechanism for pure Ni samples, while with the addition of 0.1 mole fraction or 0.2 mole fraction of Au, CNFs were formed via a tip growth mechanism at 520 °C. Single-walled CNTs formed at temperatures above 600 °C in samples doped with less than 0.2 mole fraction of Au. *Ex situ* analysis via high-resolution scanning transmission electron microscopy (STEM) and energy-dispersive X-ray spectroscopy (EDS) revealed that catalytically active particles exhibit a heterogeneous distribution of Au and Ni, where only a small fraction of the overall Au content was found in the portion of each particle actively involved in the nucleation of graphitic layers. Instead, the majority of the Au was found to be segregated to an inactive capping structure at one the end of the particles. Using density-functional theory calculations we show that the activation energy for bulk diffusion of carbon in Ni reduces from ≈1.62 eV for pure Ni to 0.07 eV with the addition of small amounts (≈ 0.06 mole fraction) of Au. This suggests that the enhancement of C diffusion through the bulk of the particles may be responsible for improving the number of particles active for nucleating the 1-D carbon nanostructures and thereby the yield.

KEYWORDS: Au-doped Ni catalyst, carbon nanofibers and Carbon nanotubes, environmental scanning/transmission electron microscope (ESTEM), *in situ* dynamic imaging, catalytic chemical vapor deposition, acetylene.

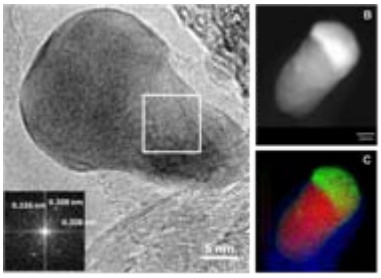

BRIEFS: (A) High resolution image extracted from a video recorded at 520 °C in 0.4 Pa of $C_2H_2$ pressure showing the inactive cap and active part for carbon nanoibers (CNFs); Fourier transform (inserted) from the boxed area confirmed the formation of $Ni_3C$ during the growth. (B) High angle annular dark-field image and (C) EDS chemical map showing that the inactive cap is Au-rich while active part of the catalyst particle is Ni-rich.

Since Haruta et al.[1] reported unexpectedly high catalytic activity of Au nanoparticles for CO oxidation at relatively low temperatures (≈70 ºC), there has been a tremendous increase in research on gold catalysis. The catalytic activity of Au is strongly related to the particle size, such that it is observed to decrease at elevated temperatures due to particle sintering and thereby decrease in the surface area. This is especially true for inactive supports ($SiO_2$, $Al_2O_3$, etc.), over which Au is known to be highly mobile. One way to reduce the mobility of Au is to use an active support, such as $TiO_2$[2] or $CeO_2$.[3] Another is to keep the Au content low by alloying it with

other metals such as Pd [4] or Pt.[5, 6] For example, an active support (e.g. ceria) improves selective reduction of a nitro group in the presence of other reducible functions,[3] while the alloying of Au with Pd improves the selective oxidation of $H_2$ to form $H_2O_2$ and of benzyl alcohol to benzaldehyde,[6]

The above-mentioned results have motivated a number of researchers to investigate the catalytic activity of Au and Au-Ni nanoparticles on various supports for the decomposition of hydrocarbons and subsequent synthesis of carbon nanotubes (CNTs).[7-11] Thus far, contradictory results have been reported for both the catalytic activity of Au for hydrocarbon dissociation and the nature of the ensuing carbon deposition. For example, the growth of single-walled CNTs (SWCNTs) from Au nanoparticles under special synthesis conditions has been reported by some groups [8, 12, 13] but Yoshihara et al. [14] found that Au had only a limited activity for CNT formation compared to Fe and Co-particles on various supports. Hsu et al. [9] showed that the addition of Au to Ni reduced the density of CNTs formed, indicating that Au inhibits CNT formation. Also, theoretical calculations predict that Au inhibits carbon deposition on Ni catalyst particles by blocking the surface steps.[15]

Encouraged by our recent successes in obtaining unambiguous insight into the CNT nucleation and growth mechanism,[16-18] we investigated the effect of doping Ni with Au on the formation of 1-D carbon structures (CNTs and CNFs) by *in situ* and *ex situ* transmission electron microscopy (TEM) techniques (high-resolution imaging, energy-dispersive X-ray spectroscopy (EDS)) and density-functional theory (DFT) calculations.

*In situ* observations of the nucleation and growth of 1-D carbon nanostructures by catalytic chemical vapor deposition (CVD) from an acetylene ($C_2H_2$) source were performed using a Tecnai F20* environmental scanning/transmission electron microscope (ESTEM) equipped with

an electron energy-loss spectrometer.[19] Au and Ni thin films (≤ 1 nm to ≈ 2 nm thick) with varying Au content (0 mole fraction (0M), 0.1 mole fraction (0.1M), 0.2 mole fraction (0.2M), 0.5 mole fraction (0.5M), 0.8 mole fraction (0.8M) and 1 mole fraction (1M)) were deposited by physical vapor deposition of pristine metals on perforated $SiO_2$ films supported on 200-mesh molybdenum TEM grids. Pure-Ni and pure-Au samples, synthesized in the same manner, were used to compare the activity of Au and Ni nanoparticles for the formation of 1-D carbon structures. These two end members of the series provided the base line for the activity of pristine nanoparticles by which to gauge the other films in the series. Samples of each film were loaded on a TEM heating holder and introduced in to the ESTEM column. TEM images from Ni films (Figure 1a) show the existence of a uniform contrast, typical of film morphology. Low-magnification scanning transmission electron microscopy (STEM) images confirmed that pure Au films dewetted from the $SiO_2$ substrate at room temperature forming 4 nm to 7 nm diameter particles while pure-Ni films balled up into 2 nm to 4 nm diameter particles only upon heating (≈ 200 ºC) (Supporting information 1A). Analyses of the Au-doped Ni specimens showed that increasing the overall Au content from 0.2 mole fraction to 0.8 mole fraction increased the extent of dewetting of the films resulting in the formation of Au nanoparticles at RT (Figure 1b-d).

Samples were held at the reaction temperature for 25 min. in order to (a) stabilize the temperature and (b) complete the reduction of any NiO to Ni in the high vacuum (≤ $10^{-4}$ Pa) of the ETEM column.[20] $C_2H_2$ was then introduced in the ESTEM sample area and a pressure of ≈ 0.4 Pa was maintained for 15 min (from here on referred to as the growth condition). Low magnification bright-field TEM images, digital video, selected-area electron diffraction patterns (SAED) and electron energy-loss spectra (EELS) were recorded from samples at room temperature (as deposited), at the reaction temperature, and after CVD. Figures 2a and 2b show

typical low-magnification images recorded from pure-Au and pure-Ni thin-film samples, respectively, after they had been subjected to the growth conditions at 520 ºC. Multiwalled carbon nanotubes (marked by arrows) were present all over the Ni samples while no carbon containing structures were observed for the pure-Au samples. The carbon-K edge is clearly present in the electron energy-loss spectra (EELS) collected from the pure-Ni samples after growth (supplementary information 1B) at the reaction temperature, and the near-edge structure is typical of the one reported for graphitic carbon.[21]. However, no such signal was observed in the spectra acquired at reaction temperature after sample Au specimen was subjected to identical growth conditions (supporting information 1B). Further *ex situ* analyses, were performed by collecting TEM images, SAED patterns and EELS data from several regions not under observation during synthesis (i.e. not exposed to electron beam under synthesis conditions), and these results confirmed that the pure Au samples were inactive for any form of C deposition.

Next, we subjected samples with varying Au/Ni atomic ratios (0.1 M to 0.8M) to the same reaction conditions as described above (details provided in the experimental section) in order to further investigate the role of Au in the formation of 1-D carbon structures. Low-magnification, room-temperature TEM images show that the dewetting of the as deposited films increased with increasing Au content in the films (Figures 1b-d). However, the particle size at the reaction temperature was not observed to change appreciably (Supporting information 1A). *In situ* digital video, recorded under reaction conditions, shows an appreciable increase in the number of tubes nucleating in the viewing region for the 0.1 M and 0.2 M samples (see supporting information 2). The samples with 0.1 mole fraction of Au contained both small and large diameter tubular structures while a more uniform tube diameter-distribution was observed for samples with 0.2 mole fraction of Au (Figure 2c and 2d, respectively). TEM images, recorded at low

magnification after the reaction, reveal the formation of an entangled network of tubular structures with catalyst particles at their tips indicating that the structures are developing via the tip-growth mechanism as observed in the videos (Figure 2c and 2d; supporting information 2). The number of tubular structures per unit area is clearly much higher for these two samples compared to that found with higher Au loadings (0.5M, and 0.8M, Figure 2e and 2f, respectively), the latter of which exhibited negligible tube formation. It is very tempting to calculate the relative activity of nanoparticles from such images, but such an approach will be subject to large uncertainties as the 2-D data available from TEM images is not sufficient to calculate particle size and density and thereby surface area with high accuracy due to the small spatial sampling. However, it is clear that low levels of Au doping in Ni increases both the linear growth rate and number of tubes formed.

Au doping also affected the growth mechanism and structure of the resulting tubes. High-resolution images and video data revealed the formation of multiwalled tubes by the root growth mechanism with a low defects density for pure Ni catalyst samples at 520 °C (inset in Figure 2b). However, tubes with 'herring-bone' (cones) and 'bamboo' structures formed by the tip-growth mechanism for samples containing 0.1 mole fraction and 0.2 mole fraction of Au (inset in Figure 2d, Supporting information 2). Similar growth mechanisms and structures have been observed for Ni samples during *in situ* observations, but at lower reaction temperatures (460 °C to 480 °C).[18, 22] On the other hand, a mixture of multi-walled and single-walled carbon nanotubes formed when the Ni thin films with 0.2 mole fraction of Au were heated to temperatures above 600 °C. Finally, at 800 °C, samples with the same overall composition produced straight SWCNTs which grew parallel and perpendicular to the beam direction as shown in Figure 2g. This differs from our previous observations using a pure Ni catalyst, where the transition to

mostly SWCNTs occurred at lower temperature (600 °C).[17] Our current results indicate that, whereas Au doping increases the catalytic activity of Ni nanoparticles, it also increases the reaction temperature for 1-D nanostructure formation.

The presence of Au in catalytically active nanoparticles was further confirmed by *ex situ* EDS data collected from the samples with two different nominal compositions in STEM mode, and typical images obtained are shown in Figure 3. A contrast difference at the tip and surface of the catalyst particles in the high-angle annular dark field (HAADF) STEM images indicated a heterogeneous distribution of Ni and Au within the particle where heavier Au-rich areas are brighter compared to Ni-rich regions (Figure 3a) due to the atomic number dependence of high-angle electron scattering. Elemental maps were obtained using EDS spectrum imaging in conjunction with principle component analysis (PCA), which identified three significant components as shown in Figure 3. The first of these was Ni-rich (Figure 3b) and was concentrated at the center of the catalyst particle, while the second was Au-rich (Figure 3c) and was present mostly at the surface of the particle. The latter component contained two distinct areas, the first of which describes a thin Au-rich layer surrounding the Ni-rich core in the lower half of the particle, while the second area was larger and was present only at one end of the elongated particle which extended outside of the C nanostructure itself (Figure 3d). The third, C-rich region was associated with the CNT grown from the particle, emphasized by blue color in Figure 3d.

A fast-Fourier transform (FFT or diffractogram) from the area marked A, in a typical high-resolution HAADF, (Figure 4, inset a) shows spots characteristic of both Au{111} (0.236 nm) as well as Ni{111} (0.204 nm) lattice spacings. In contrast, an FFT obtained from the area marked B shows the presence of predominantly Ni{111} lattice fringes. However, the existence of bright

nanoscale features on the surface of the particle in the HAADF image indicates the presence of Au nanoclusters (supporting information 1C). These results agree with the density functional theory (DFT) calculations reporting the migration of Au atoms from the center of the Ni particle to the surface. [23]

These observations were further confirmed by SAED patterns collected from the samples at room temperature (RT), during heating, and after CVD. Broad diffraction rings corresponding to Ni-111 (0.204 nm) and Ni-200 (0.179 nm) lattice spacings, respectively, were present in as-deposited Ni films (Figure 5a). The formation of nanocrystals after dewetting of the film at 520 °C resulted in the presence of rings with sharp spots (figure 5b). The diffraction ring at 0.35 nm, corresponding to the graphite-111 lattice spacing for CNTs, appears after the sample has been subjected to reaction conditions (Figure 5c), which is consistent with the previously discussed EELS data. The diffraction patterns from the samples containing 0.2 mole fraction of Au were observed to follow a similar pattern, except for the appearance of extra diffraction spots with 0.225 nm lattice spacing (Figure 5d). These spots could not be definitively indexed as either the Ni or Au structure but could be indexed as the {110} lattice-spacing from the $Ni_3C$ structure. Further evidence for the formation of $Ni_3C$ during growth was obtained from the high-resolution images extracted from a video sequence as shown in Figure 5e. A FFT from the boxed area marked in the image (inset in Figure 5e) could be unambiguously indexed as originating from the $Ni_3C$ structure. Although Ducati et al. [24] have reported the existence of a nickel-carbide structure from high-resolution images of CNT samples, generally it has not been observed. $Ni_3C$ has been reported to form as a meta-stable compound between 200 °C[25] and 265 °C[26] and to decompose above 300 °C.[27] We believe that we can observe this meta-stable phase if our experimental conditions are under a dynamic equilibrium for the following reaction:

$$3Ni + C \leftrightarrow Ni_3C$$

where the continuous flux of carbon, generated by decomposition of $C_2H_2$, favors the formation of $Ni_3C$ while the high temperature (> 520 °C) favors its decomposition. Similarly, the formation of iron carbide ($Fe_3C$) during CNT synthesis from Fe catalyst nanoparticles has also been reported.[28, 29] It is not surprising that metal carbides form prior to the CNT growth as the high carbon affinity of 3d transition metals is reflected by their low enthalpy of carbide formation.[30] Ni et al. have reported a direct relationship between CNT formation and metal carbide decomposition temperature for Ni, Co, and Fe catalysts.[31] Our observations confirm that metal carbide formation precedes the CNT or CNF nucleation and may be an intermediate step. However, the catalytic activity of these metal carbides for hydrocarbon dissociation is yet to be confirmed.

As we know, 1-D carbon nanostructure formation by CVD is a multi-step process: (1) a carbon precursor, such as $C_2H_2$, is adsorbed and decomposed on the catalyst surface; [32] decomposed carbon atoms diffuse on the surface or through the bulk of catalyst particle; [20] carbon atoms join to form graphene layers; [32] [32] these layers convert into 1-D structures such as CNFs and CNTs. Therefore, increasing the rate of these steps (or at least the rate-limiting one) will result in improving the activity/yield of carbon nanostructure formation. Our previous results have shown that the fraction of the carbon consumed for the measured CNTs growth rates for pure Ni catalyst particles is less than 0.039, of the available carbon flux (with a mean value of 0.024 ± 0.01), from which we infer that the 1$^{st}$ step is not the rate limiting step for Ni.[17] Moreover, experimental results and theoretical calculations have shown that the addition of Au to a Ni surface reduces the acetylene decomposition rate,[7, 11, 23] so we can also rule out the

possibility that Au doping improves the first step and further confirm that it is not the rate limiting.

In the past, it has been proposed that CNT nucleation and growth follows the vapor-liquid-solid (VLS) nucleation and growth process, where C diffusion through the liquid catalyst particle will be thermodynamically favorable ($2^{nd}$ step).[33] However, our observations (Supporting information 2) confirm the earlier *in situ* TEM reports that in spite of the high mobility of the catalyst particle, it is solid (crystalline) during the formation of 1-D carbon structures.[18, 22, 29, 34] Therefore carbon diffusion either on catalyst surface or in the bulk or both must be considered for crystalline particles. The surface diffusion barrier for Ni{111} and Ni{110} surface is calculated to be 0.5 eV and 0.4 eV respectively.[35, 36] For bulk diffusion, Siegel and Hamilton have shown that interstitial C in Ni favors the octahedral site over the tetrahedral site, as it is 1.59 eV lower in energy. [37] The diffusion path from one octahedral site to another octahedral site with the lowest energy barrier passes through a tetrahedral site, so the difference in energies between these two sites is the diffusion energy barrier, and the reported values in the literature for C bulk diffusion in Ni vary between 1.59 eV and 1.7 eV.[22, 35-37] As these values are much higher than for surface diffusion (0.5 eV and 0.4 eV for 111 and 110 surface, respectively), surface diffusion has been accepted as the energetically favorable diffusion path for C in a Ni catalyst.[22, 36]

Based on Siegel and Hamilton's argument we can deduce that carbon bulk diffusion will be favored in a metal lattice only if the energy for C in tetrahedral sites is equal to or nearly equal to that for the octahedral site. The energy for these two sites is very much dependent on the nature of the metal. For example, the energy for a C atom to move from an octahedral to a tetrahedral site in a bcc-Fe lattice is lower (0.86 eV) compared to that for fcc-Ni (1.59 ev – 1.7 eV).[37, 38]

In this context, it is interesting to note that Fe is also one of the preferred catalysts for obtaining a high-density of CNTs, i.e. for forest growth.[39, 40] By comparing the Ni and Fe catalyst system we can assume that the lower barrier for C bulk diffusion in Fe increases the number of active particles for CNT synthesis. Since Au doping in the Ni catalyst also improves the density of CNTs formed, it is possible that inclusion of Au in Ni nanoparticles enhances the rate of C diffusion through the bulk in the metal lattice (step 2).

To test the hypothesis, we modeled the energy barriers between C in tetrahedral and octahedral sites in pure-Au and various Au-Ni clusters using a supercell constructed from 2x2x2 perfect crystal fcc cells with a total of 32 atoms. In some cases a 3x3x3 supercell with 108 atoms was also used. The energies were calculated using the Vienna *ab initio* simulation package (VASP) density functional code using the generalized gradient approximation-projector-augmented wave (GGA-PAW) pseudopotentials.[41] A 3 x 3 x 3 grid was used for k space sampling and total energies were converged to $10^{-6}$ eV. For pure gold the octahedral site was lower in energy than the tetrahedral site by 0.16 eV. This is a very low barrier for diffusion suggesting that C bulk diffusion in pure Au may be quite fast.

Our calculations suggest that Au and Ni do not form an alloy but segregate into separate phases, and this is consistent with reports of previous calculations.[42] Using GGA we found that the $Ni_3Au$ ordered alloy has 1.0 eV per atom higher energy than the segregated phases, while local density approximation (LDA) calculations suggest that it is only 0.35 eV higher in energy when using the PAW potentials. In addition clusters of Au in Ni, as we observed using STEM imaging (Figure 3), might be stabilized by the presence of the C impurity. To explore these possibilities, we investigated a range of clusters with between 1 and 12 Au atoms in either the 2 x 2 x2 or 3x 3 x 3 Ni supercells.

We found three possible stable configurations, based on a single C atom octahedrally coordinated by 6 metal atoms. The first of these consisted of a single Au atom among the 6 metal atoms (1Au-5Ni), another with two Au atoms among the 6 metal atoms (2Au-4Ni), and finally a configuration where all 6 metal atoms octahedrally coordinating the C atom were Au (6Au) (Supplementary information 1D). In the tetrahedral configurations, all the nearest neighbors were Ni except in the case where C is octahedrally coordinated by Au atoms only and when two of the nearest neighbors were Au (Supplementary Information 1D and Table 1). Even one Au atom among the six atoms coordinating C in the octahedral site lowers the energy barrier for C diffusion substantially from 1.59 eV to 0.74 eV. In the configurations with 2 Au atoms, the tetrahedral site is slightly lower in energy (-175.34 eV) than the octahedral site (-175.41 eV). Diffusion then proceeds from one tetrahedral site to another via an octahedral site. The calculation for the case where the octahedral site is entirely surrounded by Au (6Au) indicates that there is reasonable convergence with respect to the size of the supercell, but there is still a large barrier for C diffusion (1.21 eV, Table 1).

These calculations show that the C bulk diffusion barrier is the lowest for ≈ 0.06 mole fraction of Au in Ni. As discussed previously, ex-situ characterization of active particles showed that after CVD growth, Au and Ni are heterogeneously distributed within the metal particles (Figure 3, 4 and SI # 1C). From the HAADF intensity, which carries atomic number dependence, we see that there is a Au-rich cap region in the active particle (Figure 3c). This region extends beyond the C nanostructure itself, suggesting that it is inactive for nanotube nucleation. In addition, Au rich regions are also present on the surface (Figure 4) of the particles in the part that is enclosed by the C nanostructure (i.e. the active region for the nucleation of graphitic structures). The relative size of these regions suggests that only a fraction of the overall Au content may be

present in the active part of the catalyst particles (Figure 3d). To assess the degree of segregation, we have semi-quantitatively analyzed the EDS data acquired from the Au-Ni particles, using Au-$L_\alpha$/Ni-$K_\alpha$ X-ray peak intensity ratios from different regions. This analysis indicates that in the catalytically active part of the particles (Ni rich region, Figure 1b) the Ni/Au ratio is ≈ 7 times larger than the inactive portion (Au rich region, Figure 1c). Moreover, this ratio increases to ≈ 10 times larger if the surface layer is excluded and only the central part (marked as square in Figure 3b) of the lower part of the particle is considered. This suggests that the surface of the active region is further enriched with Au rich compared to the central part, which is consistent with the STEM image contrast discussed previously. Assuming that the overall Au-content in the particle is the nominal loading of 0.2 mole fraction, the Au content in Ni rich regions will be between ≈ 0.08 (within the square marked in Figure 1c) and 0.09 (overall active region). These values agree well, within the error of the measurements, to the calculated values that will favor bulk diffusion of C (0.06 mole fraction). We can therefore explain the increased activity for CNF or CNTs formation observed here by the low barrier for C bulk diffusion in the Au doped Ni sample. As we know the Ni surfaces play an important role in dissociating hydrocarbons and Au is reported to be inactive for hydrocarbon dissociation and carbon deposition,[11] i.e. Au doping does not improve C formation, so it must improve C incorporation in the catalyst to form a carbide that in turn promotes the formation of CNTs and CNFs.

In conclusion, we show that the overall activity of Ni catalyst particles, i.e. the number of particles active for tube formation, is improved by the addition of a small amount (below 0.2 mole fraction) of Au. Although most of Au segregates to form Au rich cap, a small amount of Au is present in the active region of the particles. The addition of Au to Ni increases the temperature for the formation of carbon nanofibers with a ‘herring bone’ structure and CNTs. It also

increases the temperature for tip- growth to 600 $^{o}$C compared to 480 °C for pure Ni. We also show that the structure of the catalyst particle is $Ni_3C$ during growth instead of fcc-Ni that has been assumed up to now. We believe that carbides are observed due to the dynamic equilibrium conditions present under the reaction condition. Based on our DFT calculations, we propose that small levels of Au doping increases the number of particles active for CNF and CNT formation, resulting in higher yield, due to the negligible energy barrier (0.07 eV) for C bulk diffusion compared to pure Ni (1.62 eV).

ACKNOWLEDGMENT Financial support from NSF-CBET#0625340, assistance of Mr. Karl Weiss and Stefano Mazzucco for experimental set up, and the use of ESTEM at John Cowley Center for High Resolution Electron Microscopy at Arizona State University is gratefully acknowledged.

**DISCLAIMER:** ***The full description of the procedures used in this manuscript includes identification of certain commercial products and their suppliers. The inclusion of such information should in no way be construed as indicating that such products or suppliers are endorsed by NIST or are recommended by NIST or that they are necessarily the best materials, instruments, software or suppliers for the purposes described.***

SUPPORTING INFORMATION PARAGRAPH

**Experimental**: 1 nm to 2 nm of thin metal films of varying compositions were deposited on perforated $SiO_x$ thin films supported on Mo TEM grids. Mo grids were chosen due to their high melting point (2623 ºC) compared to the growth temperature. Samples were loaded in a TEM holder equipped with a heating furnace and inserted in ETEM column. Low- and high-magnification TEM and STEM images, selected area electron diffraction (SAED) patterns and

electron energy-loss spectroscopy (EELS) data from several regions were recorded at room temperature. The same set of data was also collected after heating the samples to growth temperature of 520 °C, 600 °C and 800 °C in vacuum ( $10^{-4}$ Pa). Samples were held at the growth temperature for 20 min to 25 min to stabilize the temperature and to reduce the sample drift. 0.4 Pa of $C_2H_2$ was then introduced in the sample region of the ETEM and digital video of the nucleation and growth process was recorded at the rate of 15 frames $s^{-1}$. TEM images and SAED patters from various regions were also recorded under reaction conditions. $C_2H_2$ flow was stopped after 15 min and the sample area was evacuated back to the high vacuum condition. EELS data was collected under high vacuum conditions in order to avoid the contribution of the C signal from the gas to the signal from the sample. Samples were then stored and further analyzed to make sure that electron beam did not affect our *in situ* observations. Energy-dispersive X-ray spectroscopy (EDS) was also collected, *ex situ*, using a probe corrected TEM/STEM.

Supporting Information:

1A. Typical electron energy loss spectra collected after carbon nanostructure growth from (top) pure Ni, (center) Ni with 0.2 mole fraction of Au, and pure Au samples. Background subtracted C-K edge showing the sharp pre-edge feature, also known as the pi* peak that is indicative of a graphitic structure, is inset in the upper left hand corner for each spectrum.

1B. Annular dark-field (ADF) images recorded in STEM mode from Ni thin film samples containing 0.1 mole fraction of Au showing that Au nanoparticles (bright particles marked by arrows in the top left) are present in as deposited films. Nickel particles, less intense than Au due to their lower atomic number, can be seen in the sample heated to 200 °C. Au particle size does

not change appreciably upon further heating up to 520 °C but the intensity from the Ni particles increases. Au and Ni co-exist in some of the particles after CNT growth. Note that the shape of the particle also changes during growth (Lower right panel).

1C. High-angle annular dark-field (HAADF) images recorded *ex situ* after carbon nanostructure growth from the Ni sample containing 0.2 mole fraction of Au showing the distribution of higher intensity in the images due to Au. Note the existence of nano-size Au-rich regions in the circled areas along with large Au rich regions in both images.

1D. Atomic models used for DFT calculations showing the location of carbon in tetrahedral and octahedral sites for (left pair) 1 Au atom and 31 Ni atoms, (central pair) 2 Au atoms and 30 Ni atoms, and (right pair) 6 Au and 26 Ni atoms. Note that the activation energy for carbon to move from the octahedral to tetrahedral position progressively decreases from left to right.

Video-1. Digital video recorded at the rate of 15 frames $s^{-1}$ from 0.2 mole fraction of Au in Ni at 520 °C in 0.4 Pa of $C_2H_2$, Note multiple particles being active in forming 1-D nanostructure simultaneously.

FIGURE CAPTIONS

Figure1. Low magnification TEM images recorded at room temperature (RT) from as-deposited films. (a) Pure Ni films have almost uniform contrast that is typical of continuous film morphology, (b) small particles, formed by dewetting, can be seen in the film with 0.2 mole fraction Au. (c-d) The extent of dewetting and thereby formation of well defined particles at RT increased as the Au content in Ni films increased from (c) 0.5 mole fraction to (d) 0.8 mole fraction.

Figure2. Low-magnification images recorded at room temperature after the samples have been heated to 520 °C and exposed to 0.4 Pa of $C_2H_2$ for 15 min to 20 min (growth condition). (a) Pure Au, (b) pure Ni with high resolution image showing multi-walled CNTs that typically formed during growth condition, (c) 0.1 mole fraction of Au in Ni, (d) 0.2 mole fraction of Au in Ni, high resolution image of typical 1-D nanostructures formed during growth in inset in lower right hand corner (e) 0.5 mole fraction of Au in Ni, and (f) 0.8 mole fraction of Au in Ni. (g) HREM image showing formation of SWCNTs (arrows mark the tubes growing perpendicular to the image plane) at 800 °C for 0.2 mole fraction Au in Ni sample. Note the density of 1-D nanostructure is a maximum for samples with 0.1 mole fraction and 0.2 mole fraction of Au. Also, the Au doping level mentioned is the overall content in the starting thin films.

Figure3. (a) Dark-field STEM images from 0.2 mole fraction of Au in Ni sample, recorded *ex situ* after growth, and results of PCA of EDS spectrum image showing (b) Ni-rich, and (c) Au-rich component images. (d) A color overlay (d) emphasizes the spatial extent of each of these components (red = Ni-rich, green = Au-rich, blue = C-rich). Note that the signal associated with the C nanostructure only surrounds the Ni rich region. Bar is 10 nm.

Figure4. HAADF image showing the co-existence of Au, mostly on the surface, and Ni in the bulk as confirmed by the FFT's (diffractogram) obtained from regions marked A and B (inset in the bottom right and top left corner) respectively. Bar is 10 nm.

Figure5. Selected area electron diffraction (SAED) patterns from pure Ni thin films recorded at (a) room temperature, (b) at 520 °C and (c) at room temperature after growth. (d) SAED at room temperature after growth from 0.2 mole fraction of Au in Ni is included for comparison. Arrows indicate the presence of a 0.224 nm spacing that can be indexed as the {110} spacing from $Ni_3C$.

(e) FFT pattern (inset in lower left hand corner) from the boxed area marked in the high-resolution image extracted from a video sequence during growth was indexed using $Ni_3C$ structure.

References:


1. Haruta, M., Kobayashi, T., Sano, H., Yamuda, N., *Novel Gold Catalysts for the Oxidation of Carbon Monoxide at a Temperature far Below 0°C.* Chem. Lett., 1987. **2**: p. 405–408.
2. Lin, S.D., M. Bollinger, and M.A. Vannice, *Low-Temperature CO Oxidation Over $Au/TiO_2$ and $Au/SiO_2$ Catalysts.* Catalysis Letters, 1993. **17**(3-4): p. 245-262.
3. Corma, A. and P. Serna, *Chemoselective hydrogenation of nitro compounds with supported gold catalysts.* Science, 2006. **313**(5785): p. 332-334.
4. Enache, D.I., Edwards, Jennifer K., Landon, Philip, Solsona-Espriu, Benjamin, Carley, Albert F., Herzing, Andrew A., Watanabe, Masashi, Kiely,Christopher J., Knight, David W., Hutchings, Graham J. , *Solvent-Free Oxidation of Primary Alcohols to Aldehydes Using Au-Pd/ $TiO_2$ Catalysts.* Science, 2006. **311**: p. 362-365.
5. Dimitratos, N.V., A., Wang, D., Porta, F. Su, D.S., Prati, L., *Pd and Pt catalyst modified by alloying with Au in selective oxidation of alcohols.* Journal of Catalysis, 2006. **244**(1): p. 113-121.
6. Xu, J.B., Zhao, T.S., Li, Y.S., Yang, W.W., *Synthesis and Characterization of the Au-modified cathode catalyst for alkaline direct ethonol fuel cells.* International Journal of Hydrogen Energy, 2010. **35**(18): p. 9693-9700.
7. Molenbroek, A.M., J.K. Norskov, and B.S. Clausen, *Structure and reactivity of Ni-Au nanoparticle catalysts.* Journal of Physical Chemistry B, 2001. **105**(23): p. 5450-5458.
8. Bhaviripudi, M., S., E., Steiner III, S. A., Zare, A. T., Dresselhaus, M. S., Belcher, A. M., Kong, J., *CVD Synthesis of Single-Walled Carbon Nanotubes from Gold Nanoparticle Catalysts.* Journal of American Chemical Society, 2007. **129**: p. 1516-1517.
9. Hsu, C.H., Chen, C.F., Chen, C.C., Chan, S.Y., *Density-controlled carbon nanotubes.* Diamond and Related Materials, 2005. **14**(3-7): p. 739-743.
10. Lee, S.-Y., Yamada, M. Miyake, M., *Synthesis of carbon nanotubes over gold nanoparticle supported catalysts.* Carbon, 2005. **43**: p. 2654–2663.
11. Vang, R.T., et al., *Controlling the catalytic bond-breaking selectivity of Ni surfaces by step blocking.* Nature Materials, 2005. **4**(2): p. 160-162.
12. Yuan, D., Ding, L., Chu, H., Feng, Y., McNicholas, T.P., Liu, J., *Horizontally Alighned Single-Walled carbon Nanotube on Quartz from a Large Variety of Metal Catalysts.* Nano Letters, 2008. **8**(8): p. 2576-2579.
13. Takagi, D., Homma, Y., Hibino, H., Suzuki, S., Kobayashi, Y., *Single-Walled Carbon Nanotube Growth from Highly Activated Metal Nanoparticles.* Nano Letters, 2006. **6**(12): p. 2642-2645.

14. Yoshihara, N.A., H. Tsuji, M., *Growth Mechanism of Carbon Nanotubes over Gold-Supported Catalysts.* japanese Journal of Applied Physics, 2008. **47**(4): p. 1944-1948.
15. Besenbacher, F., Chorkendorff, I., Clausen, B. S., Hammer, B.,Molenbroek, A. M., Nørskov, J. K., Stensgaard, I., *Design of a Surface Alloy Catalyst for Steam Reforming.* Science, 1998. **279**: p. 1913-1915.
16. Sharma, R., Zafar, Iqbal *In situ observations of carbon nanotube formation using environmental electron microscopy (ETEM).* Applied Physics Letters, 2004. **84**: p. 990-992.
17. Sharma, R., Rez, Peter, Brown, Megan, Du, Gaohui, and and M.M.J. Treacy, *Dynamic observations of the effect of pressure and temperature conditions on the selective synthesis of carbon nanotubes.* Nanothecnology, 2007. **18**(12): p. 125602 (8pp).
18. Hofmann, S., Sharma, R., Ducati, C., Du, G., Mattevi, C., Cepek, C., Mirco, C., Pisana, S., Parvez, A., Cervantes-Sodi, F., Ferrari, A. C., Dunin-Borkowski, R., Lizzit, S., Petaccia, L., Goldoni, A., Robertson, J., *In situ Observations of Catalyst Dynamics during Surface-Bound Carbon Nanotube Nucleation.* Nano Letters, 2007. **7**(3): p. 602-608.
19. Sharma, R., *An environmental transmission electron microscope for in situ synthesis and characterization of nanomaterials.* Journal of Materials Research, 2005. **20**(7): p. 1695-1707.
20. P. Rez, E.S.M., and R. Sharma, Microsc. & Microanal. 14 1382CD., *In Situ Measurements of Ni Oxidation State Using Electron Energy-Loss Spectroscopy.* Microscopy and Microanalysis, 2008. **proceedings**: p. 1382CD.
21. Ahn CC, K.O., *EELS Atlas.* Arizona State University, HREM Facility and Gatan Inc., Tempe, Arizona, 1983.
22. Helveg, S., Lopez-Cartes, C., Sehested, J., Hansen, P.L.,Clausen, B.S., Rostrup-Nielsen, J.R., Abild-Pedersen, F., and Norskov J., *Atomic-scale imaging of carbon nanofibre growth.* Nature, 2004. **427**: p. 426
23. Nielson, L.P., Bessenbacher, F., Strensgaard, L., Laegsgaard, E., Engdahl, C., Stoltze, P., Jacobsen, K.W., Norskove, J.K., *Initial growth of Au on Ni(110): Surface alloyng of immiscible metals.* Physical Review Letters, 1993. **71**(5): p. 754-758.
24. Ducati, C., et al., *The role of the catalytic particle in the growth of carbon nanotubes by plasma enhanced chemical vapor deposition.* Journal of Applied Physics, 2004. **95**(11): p. 6387-6391.
25. Hooker, P., Tan, Beng J., Klabunde, Kenneth J., Suib, Steve, *Preparation of Nickel Carbide Ultrafine Particles by Metal Vapor Methods.* Chemistry of Materials, 1991. **3**(5): p. 947-952.
26. Struis, R., et al., *Studying the Formation of Ni3C from CO and Metallic Ni at T=265 degrees C in Situ Using Ni K-Edge X-ray Absorption Spectroscopy.* Journal of Physical Chemistry C, 2009. **113**(6): p. 2443-2451.
27. Hofer, L.J.E., Cohn, E.M., Peebles, W.C., *Isothermal Decomposition of Nickel Carbide.* Journal of Physical Chemistry, 1950. **54**(8): p. 1161-1169.
28. Yoshida, H., Takeda, Seiji, Uchiyama,Tetsuya, Kohno, Hideo,Homma, Yoshikazu, *Atomic-Scale In-situ Observation of Carbon Nanotube Growth from Solid State Iron Carbide Nanoparticles.* Nano Letters, 2008. **XX**.
29. Sharma, R., Moore, E.S., Rez, P, Treacy M.M.J., *Site-specific fabrication of Fe particles for carbon nanotube growth.* Nano Letters, 2009. **9**(2): p. 689-694.

30. Meschel, S.V., Kleppa, O.J., *Standard Enthalpies of formation of some 3d transition metal carbides by high temperature calorimetry.* Journal of Alloys and Compounds, 1997. **257**(1-2): p. 227-233.
31. Ni, L., et al., *Decomposition of metal carbides as an elementary step of carbon nanotube synthesis.* Carbon, 2009. **47**(13): p. 3054-3062.
32. Haruta, M., Kobayashi, T., Sano, H., Yamuda, N., . Chem. Lett., 1987. 2: p. 405–408., *Novel Gold Catalysts for the Oxidation of Carbon Monoxide at a Temperature far Below 0°C.* Chemical Letters, 1987. **2**: p. 405-408.
33. Baker, R.T.K., Barber, M.A., Harris, P.S., Feates, F.S., Waite, R.J., *Nucleation and growth of carbon deposits from the Ni catalyzed decomposition of acetylene.* Journal of Catalysis, 1972. **26**: p. 51-62.
34. Sharma, R., Rez, Peter, Treacy, M.M.J. and Stuart, Steven J. , *In-situ observation of the growth mechanisms of carbon nanotubes under diverse reaction conditions.* Journal of Electron Microscopy, 2005. **54**: p. 231-237.
35. Abild-Pedersen, F., NørskovJens, Jens K.,Rostrup-Nielsen, R., Sehested, Jens, and Helveg, Stig *Mechanisms for catalytic carbon nanofiber growth studied by ab initio density functional theory calculations.* Physical Review B, 2006. **73** p. 115419.
36. Hofmann, S., Csa´nyi, G., Ferrari, A. C., Payne, M. C., Robertson, J. , *Surface Diffusion: The Low Activation Energy Path for Nanotube Growth.* Physical Review Letters, 2005. **95**: p. 036101.
37. Siegel. D.J., H., J.C. , *First-principles study of the solubility, diffusion, and clustering of C in Ni.* Physical Review B, 2003. **68**: p. 094105(7pp).
38. Jiang, D.E. and E.A. Carter, *Carbon dissolution and diffusion in ferrite and austenite from first principles.* Physical Review B, 2003. **67**(21).
39. Goswami, S., et al., *Aligned Carbon Nanotube Stationary Phases for Electrochromatographic Chip Separations.* Chromatographia, 2009. **69**(5-6): p. 473-480.
40. Bedewy, M., et al., *Collective Mechanism for the Evolution and Self-Termination of Vertically Aligned Carbon Nanotube Growth.* Journal of Physical Chemistry C, 2009. **113**(48): p. 20576-20582.
41. Kresse, G.F., J. , *Efficient iterative schemes for ab initio total-energy calculations using a plane-wave basis set.* Physical Review B, 1996 **54**: p. 11169-11186.
42. Nielsen, L.P., et al., *Initial Growth of Au on Ni(110) - Surface Alloying of Immiscible Metals.* Physical Review Letters, 1993. **71**(5): p. 754-757.

Table 1. Energy needed for C atom to move from Octahedral to Tetrahedral site for different Au-Ni compositions

| Total Number of Atoms | Number of Au Atoms | Number of Ni Atom | Mole fraction | Carbon in tetrahedral site (eV) | Carbon in octahedral site (eV) | Energy difference between two sites (diffusion barrier, eV) |
|---|---|---|---|---|---|---|
| 32 | 1 | 31 | 0.03125 | -177.98 | -178.72 | 0.74 |
| 32 | 2 | 30 | 0.0625 | -175.41 | -175.34 | 0.07 |
| 32 | 6 | 26 | 0.1875 | -162.83 | -161.62 | 1.21* |

*With 6 Au atoms, the energy for octahedral-site is higher than for tetrahedral site.

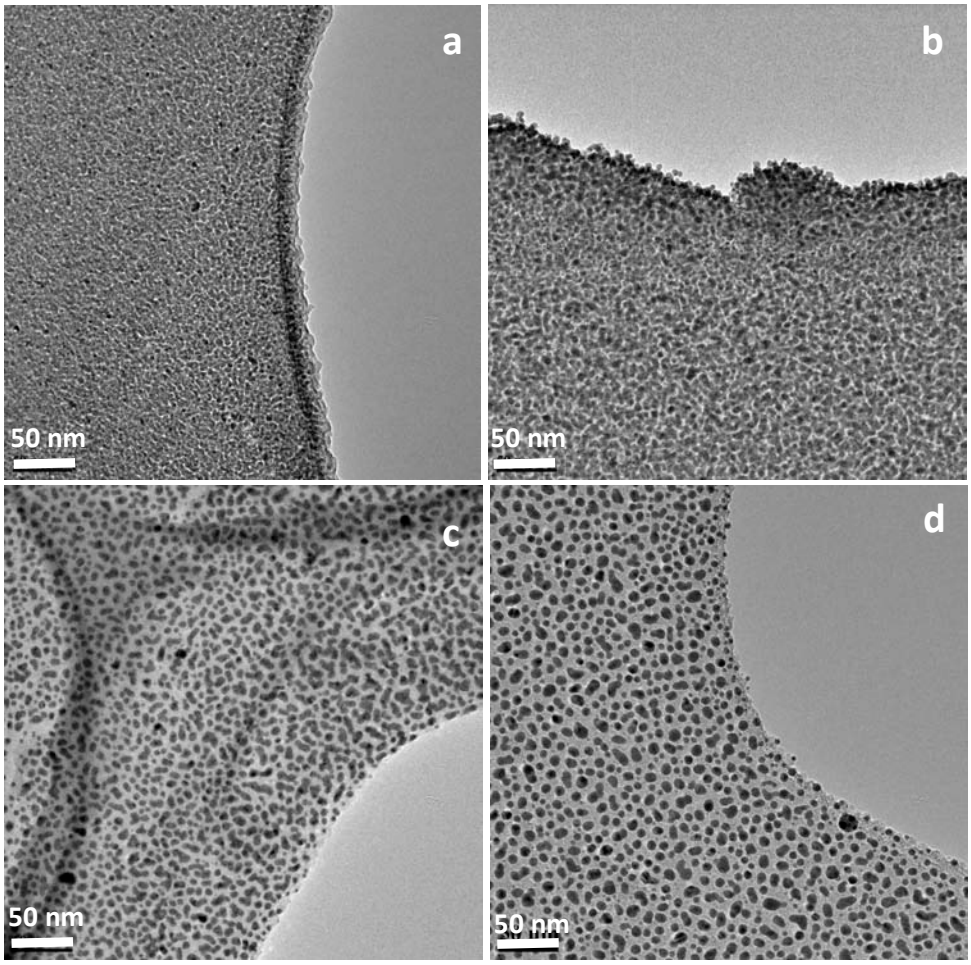


Figure 1

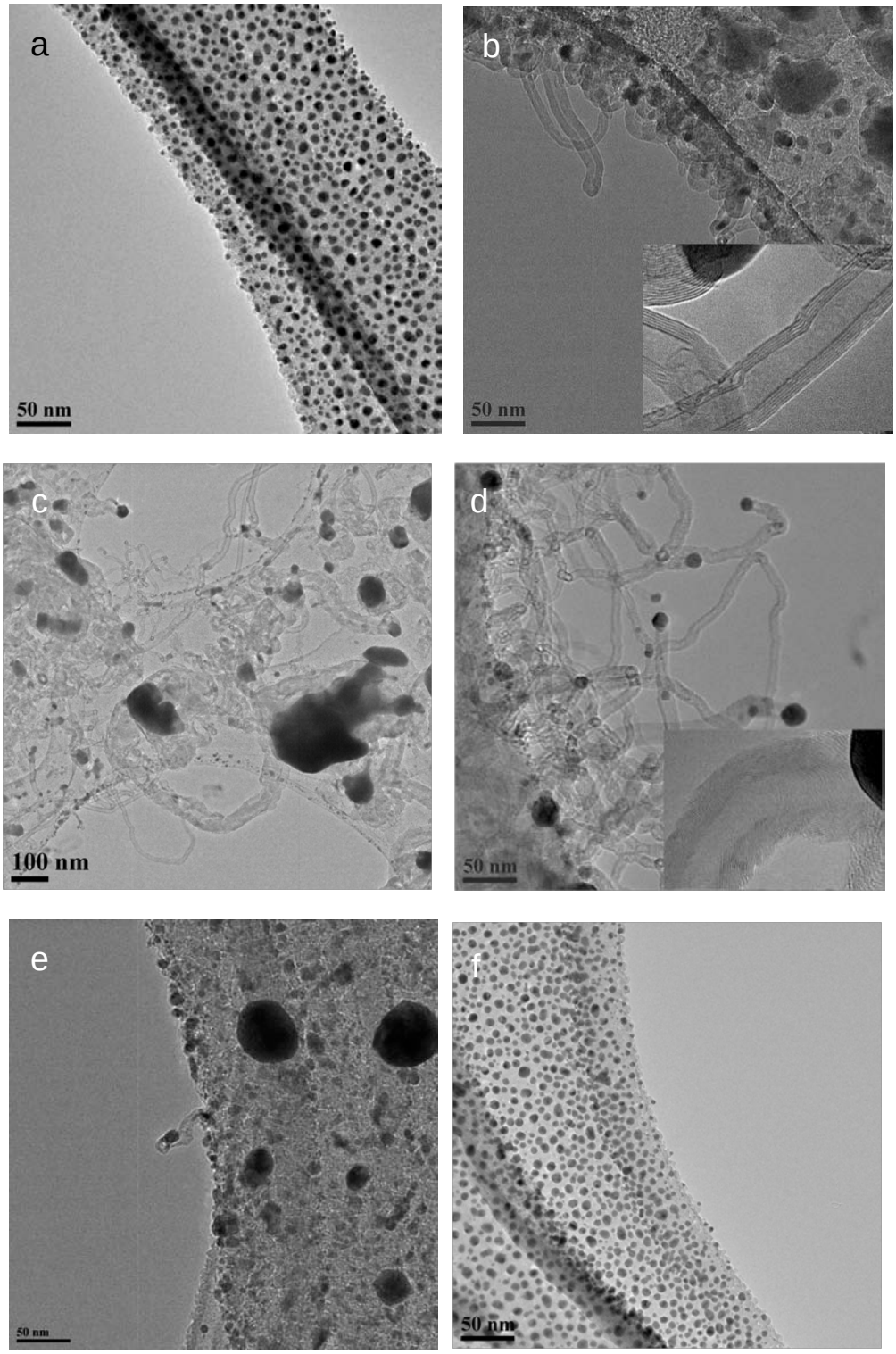
a
50 nm
b
50 nm
c
100 nm
d
50 nm
e
50 nm
f
50 nm

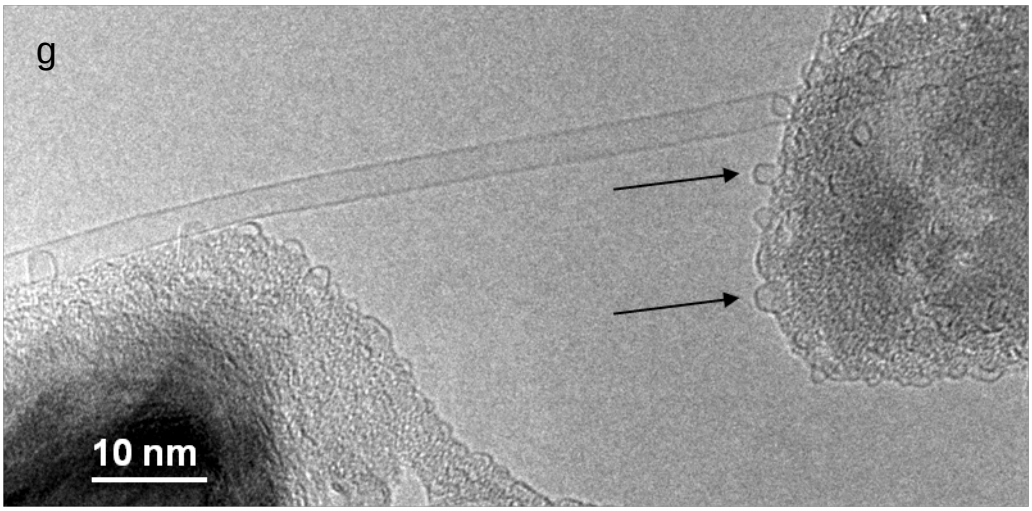


Figure 2

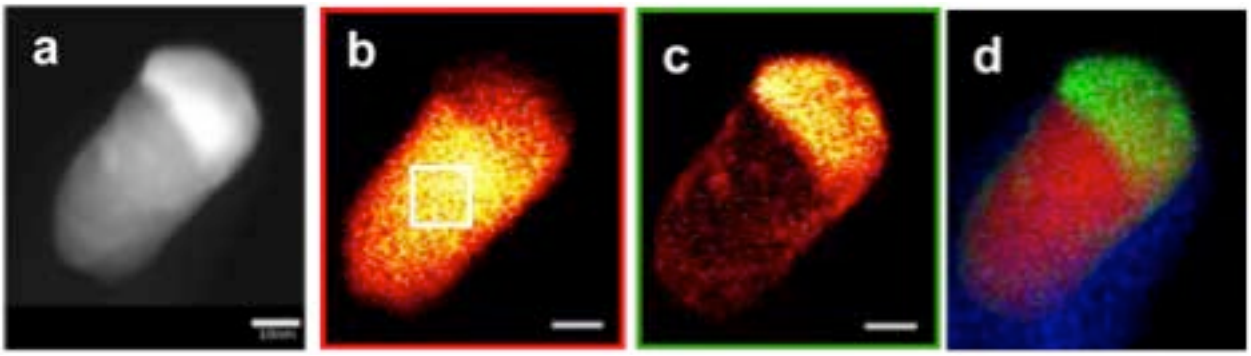


Figure 3

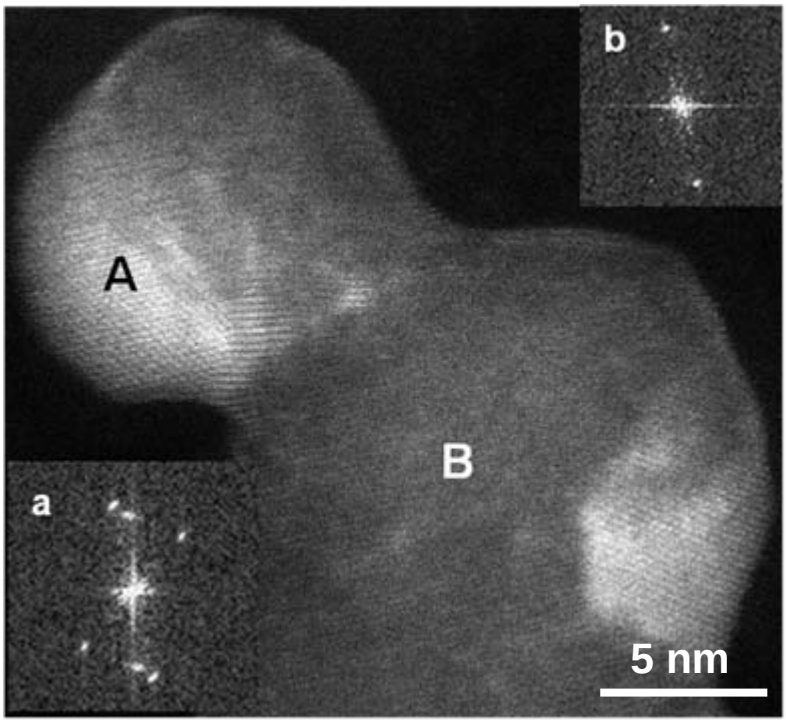


Figure 4.

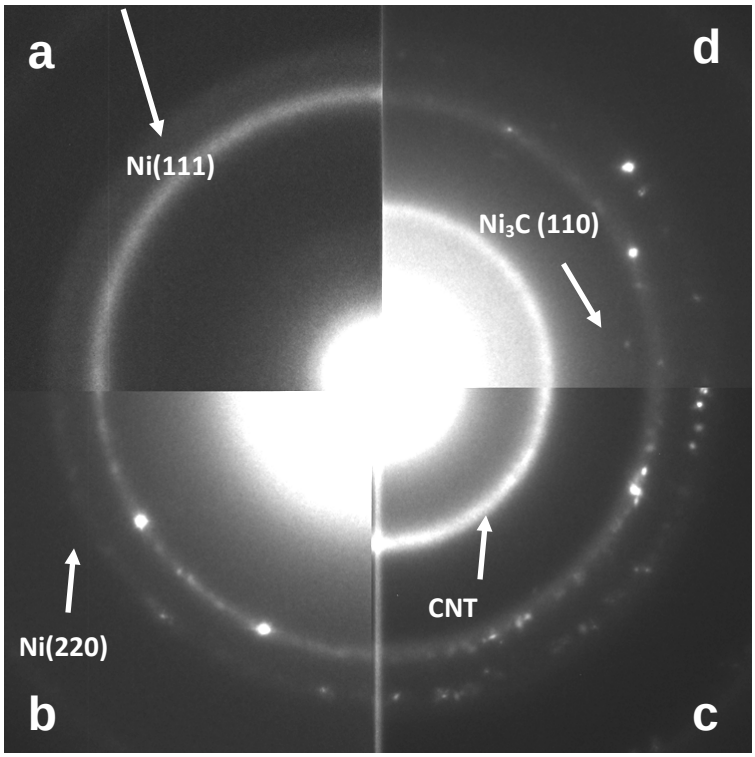


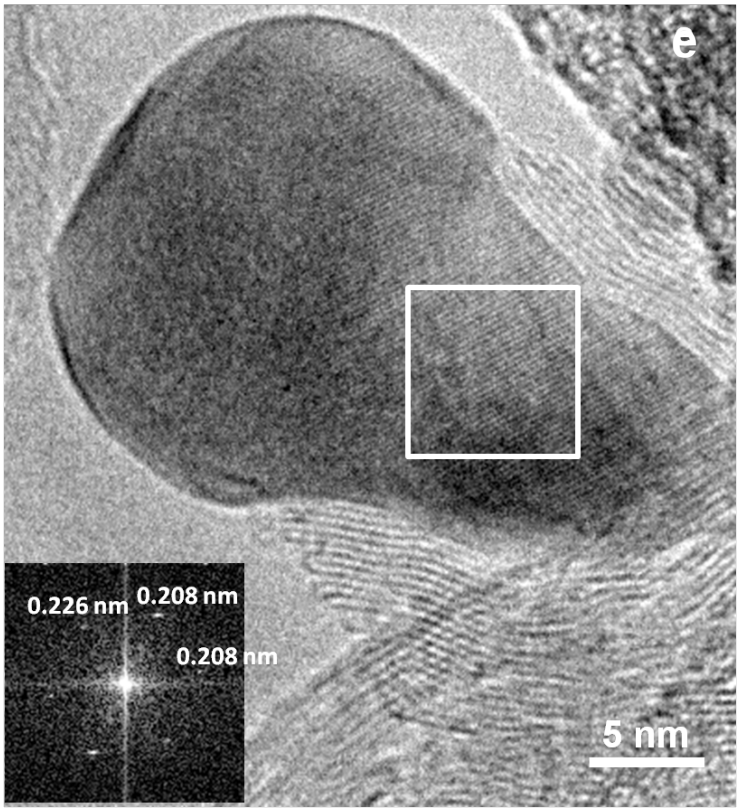


Figure 5

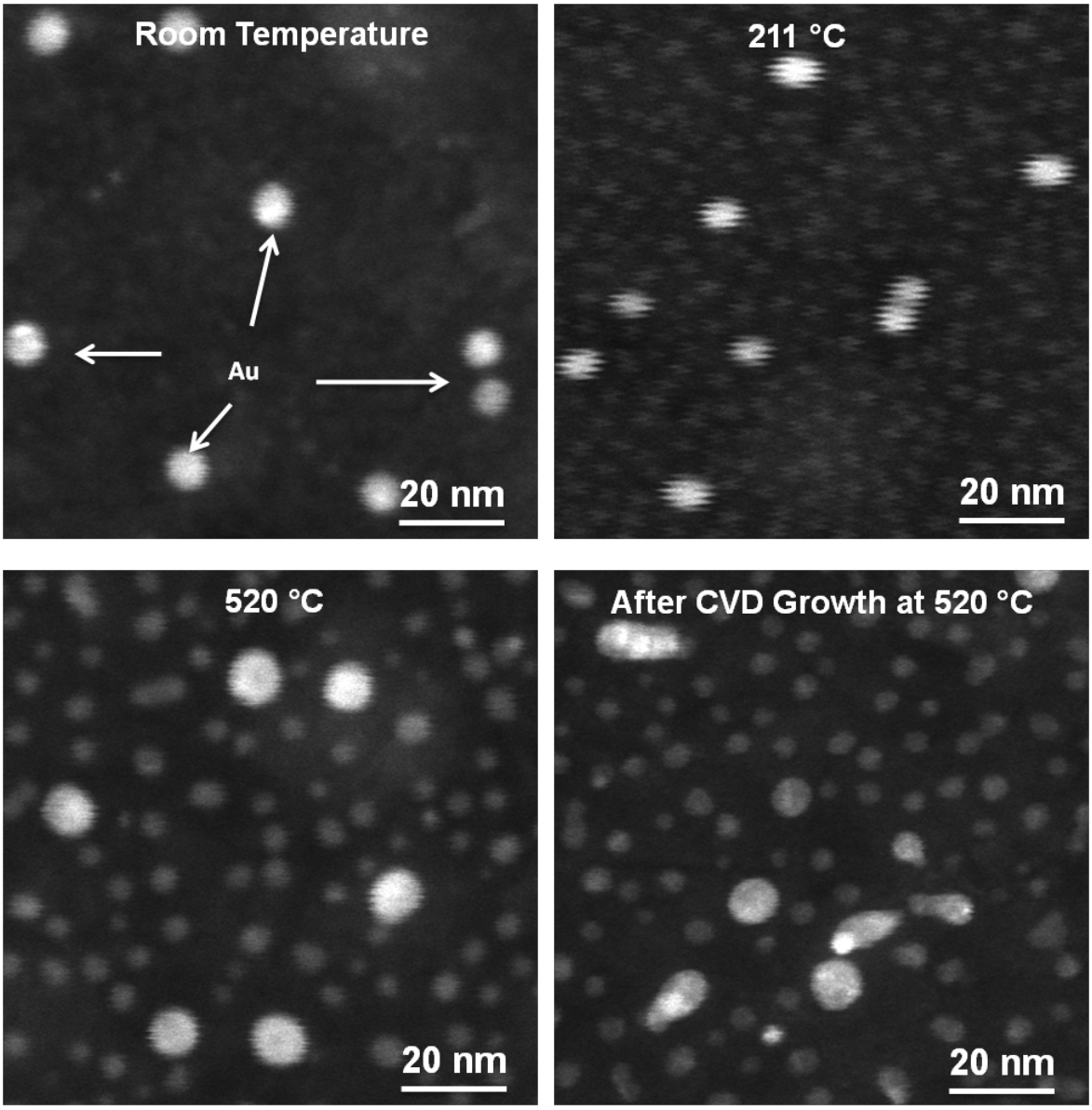


Supplementary information 1A

(Top left) Annular dark-field (ADF) images recorded in STEM mode from Ni thin film samples containing 10 atom fraction of Au showing that Au nanoparticles (bright particles marked by arrows in the top left), with an average size of 5.9 ±1.0 nm are present in as deposited films. (To right) Nickel particles with an average size of 3.8±1.0 nm, lighter than Au due to lower atomic number, can be seen in the sample heated to 211 °C. (Bottom left) Au particle size does not change appreciably upon further heating up to 520 °C but Ni particles increase slightly (4.3±1.3 nm) and become more pronounced. (Bottom right) Au and Ni co-exist in some of the particles after CNT growth. Note that the shape of the particle also changes during growth.

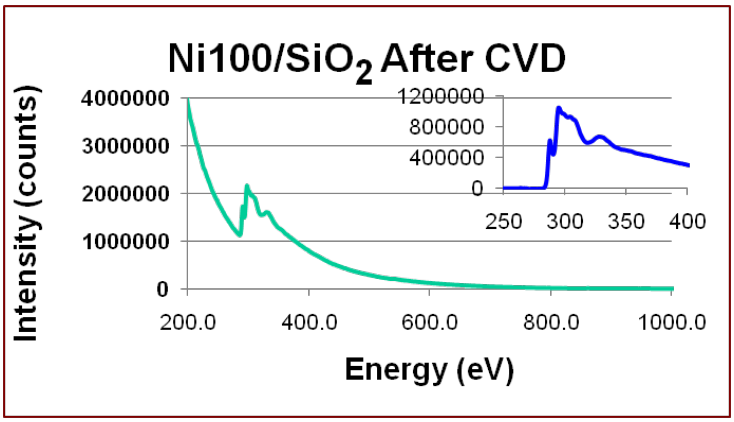


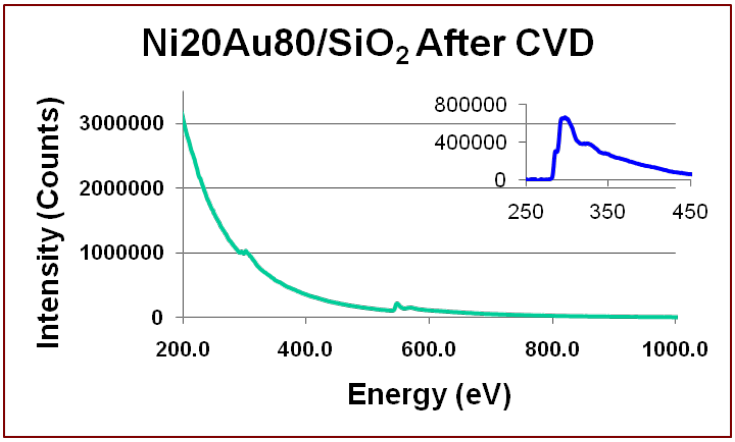


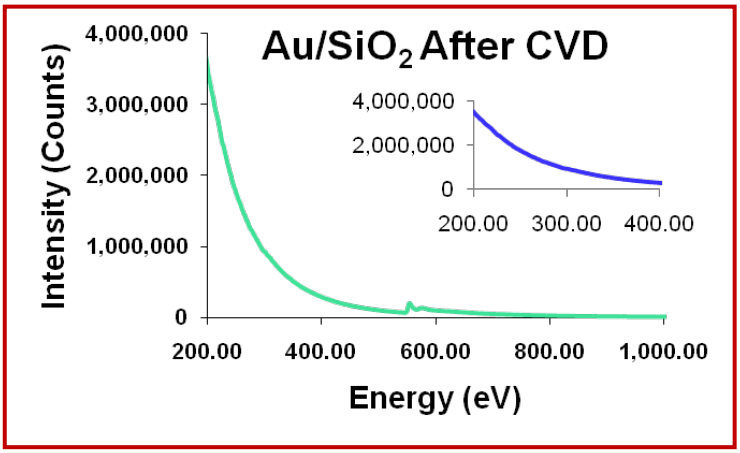


Supporting Information -1B:

Typical electron energy loss spectra collected after carbon nanostructure growth from (top) pure Ni, (center) Ni with 20 atom fraction of Au, and (bottm) pure Au samples. Background subtracted C-K edge is inset in the upper left hand corner for each spectra. Oxygen signal at 532 eV is from the support.

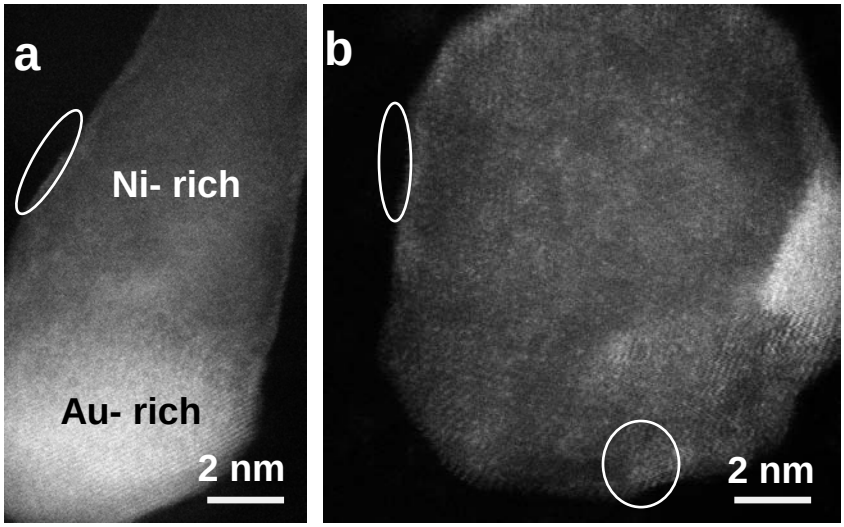


Supporting information 1C:

High-angle annular dark-field images recorded ex-situ after carbon nanostructure growth from the Ni sample containing 20 atom fraction of Au show the distribution of lighter contrast in the images due to Au. Note the existence of nanosize Au particles in the circled region along with large Au rich regions in both images.

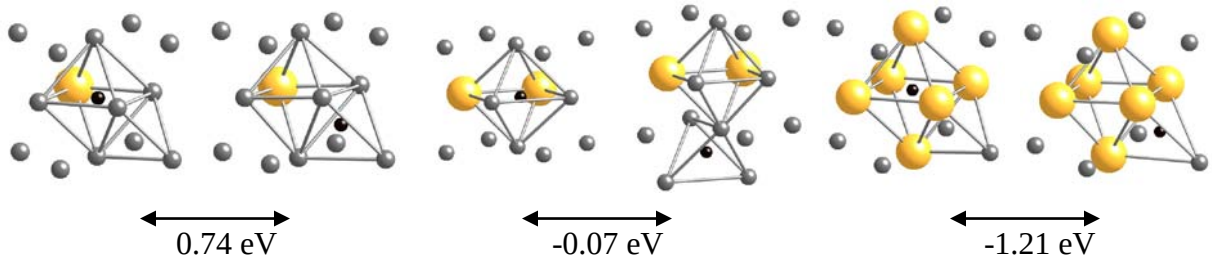


Supporting Information 1D:

Models used for DFT calculations showing C (black) in octahedral and tetrahedral sites (as marked) for 32 atom cell with (left to right) 1 Au (yellow) and 31 Ni (silver), 2 Au and 30 Ni, and 6 Au and 26 atoms respectively. Difference in energy for C stabilization between octahedral and tetrahedral sites is given below each set.